Atmospheric
Chemistry
and Physics

Supplement of

Formaldehyde and hydroperoxide distribution around the Arabian Peninsula – evaluation of EMAC model results with ship-based measurements

Dirk Dienhart et al.

Correspondence to: Dirk Dienhart (d.dienhart@mpic.de) and Horst Fischer (horst.fischer@mpic.de)
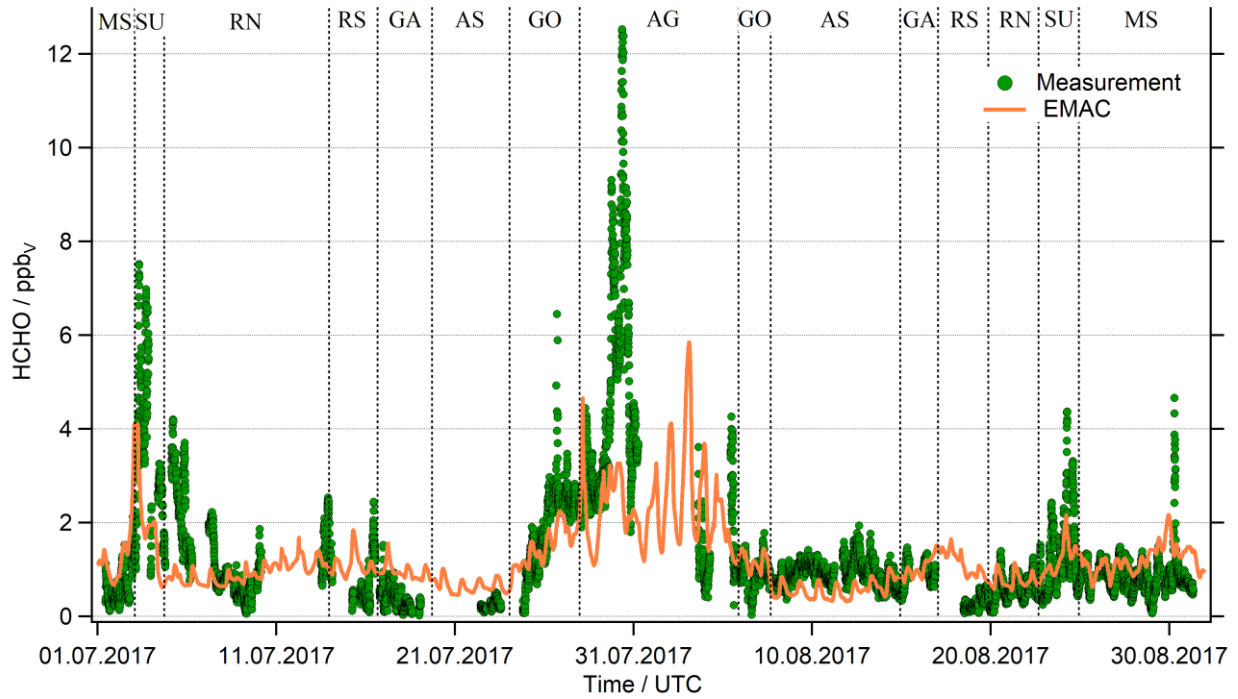
Figure S1: Timelines of the HCHO measurements and the EMAC simulation, averaged along the ship track.
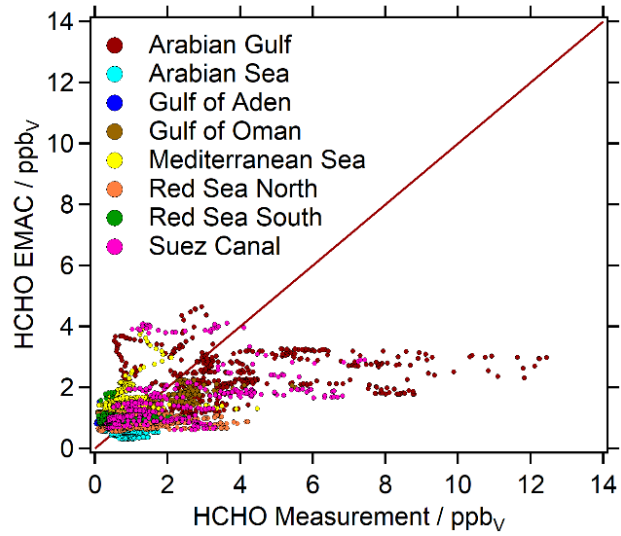
Figure S2: Scatter plot of the HCHO measurements versus the simulated data (EMAC) in hourly averages.
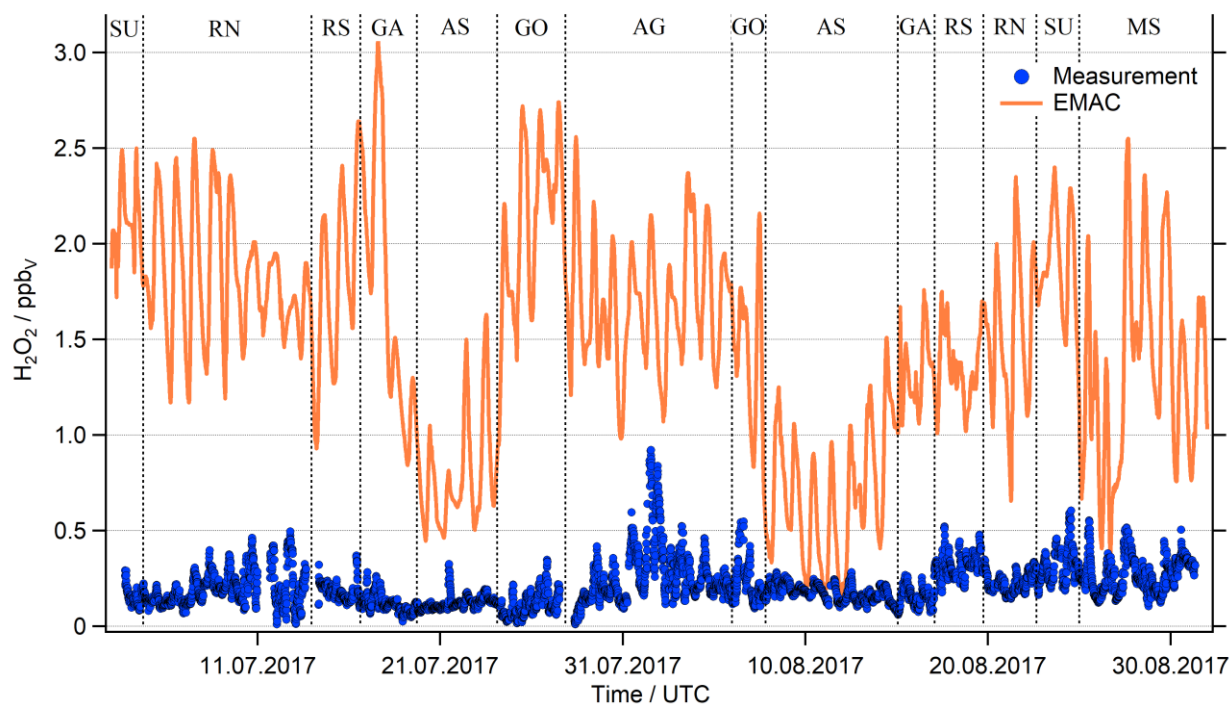
Figure S3: Timelines of the H₂O₂ measurements and the EMAC simulation, averaged along the ship track.
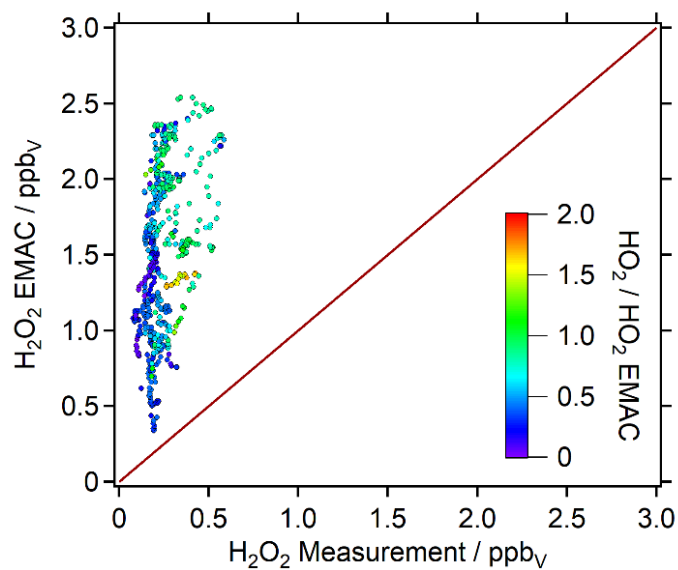
Figure S4: Scatter plot of the H₂O₂ measurements versus the simulated data (EMAC) in hourly averages.
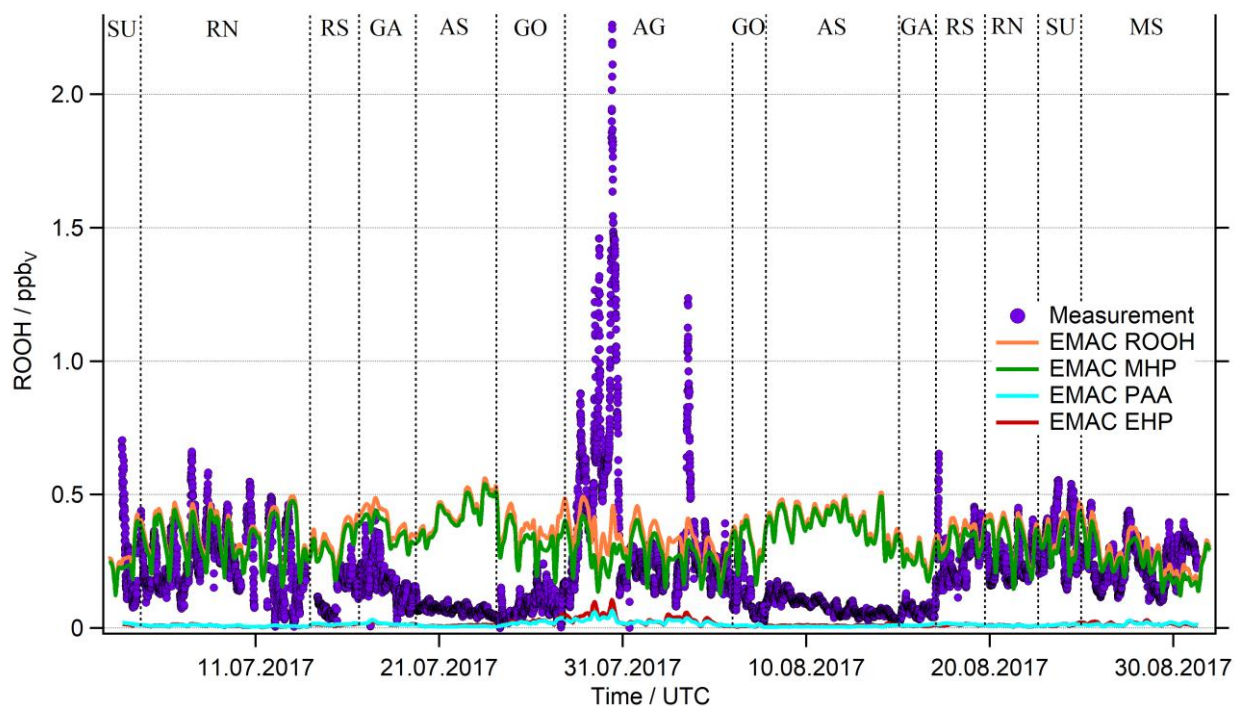
Figure S5: Timelines of the organic peroxide (ROOH) measurements and the EMAC simulations along the ship the track. The simulated dataset consists of the most prominent species methyl hydroperoxide (MHP), peracetic acid (PAA) and ethyl hydroperoxide (EHP).
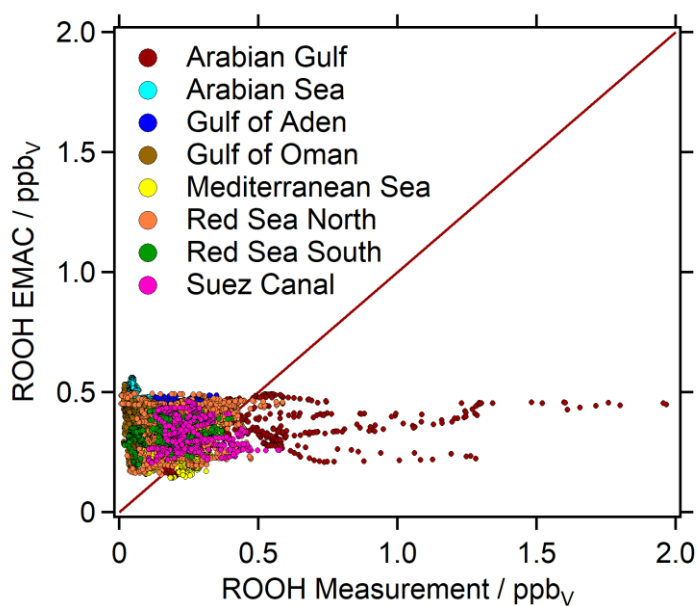
Figure S6: Scatter plot of the organic peroxide measurements versus the simulated data (EMAC) in hourly averages.

Table S1: Mean, median, 25- and 75-percentile values of the HCHO, H₂O₂ and organic peroxide measurements (black) and the corresponding EMAC simulations (orange) for the eight different regions encountered during AQABA: Mediterranean Sea (MS), Suez Canal (SU), Red Sea North (RN), Red Sea South (RS), Gulf of Aden (GA), Arabian Sea (AS), Gulf of Oman (GO) and Arabian Gulf (AG).

HCHO	MS	SU	RN	RS	GA	AS	GO	AG
Mean	0.818±0.397	2.074±1.612	1.037±0.783	0.519±0.435	0.566±0.337	0.826±0.326	1.499±0.831	3.769±2.443
±SDev	1.260±0.389	1.535±0.837	0.799±0.145	0.986±0.192	1.019±0.169	0.588±0.178	1.410±0.331	2.259±0.765
Median	0.771	1.499	0.763	0.374	0.503	0.862	1.218	3.077
	1.220	1.290	0.775	0.942	0.966	0.572	1.360	2.190
25%	0.602	0.888	0.520	0.232	0.286	0.633	0.897	2.368
	1.040	0.941	0.673	0.906	0.896	0.430	1.140	1.550
75%	0.989	2.925	1.264	0.574	0.814	1.045	2.332	4.528
	1.400	1.820	0.882	1.020	1.160	0.734	1.633	2.850
H₂O₂	**MS**	**SU**	**RN**	**RS**	**GA**	**AS**	**GO**	**AG**
Mean	0.269±0.088	0.271±0.113	0.204±0.084	0.255±0.085	0.129±0.046	0.155±0.046	0.148±0.092	0.261±0.149
±SDev	1.328±0.512	1.984±0.253	1.756±0.379	1.598±0.402	1.594±0.573	0.721±0.323	1.851±0.537	1.684±0.327
Median	0.263	0.252	0.192	0.246	0.121	0.146	0.125	0.210
	1.310	2.040	1.730	1.520	1.370	0.672	1.780	1.670
25%	0.200	0.185	0.141	0.183	0.096	0.118	0.081	0.166
	0.892	1.803	1.480	1.290	1.210	0.506	1.505	1.450
75%	0.329	0.352	0.253	0.318	0.155	0.189	0.188	0.327
	1.590	2.188	1.985	1.780	1.840	0.928	2.295	1.900
ROOH	**MS**	**SU**	**RN**	**RS**	**GA**	**AS**	**GO**	**AG**
Mean	0.216±0.069	0.270±0.094	0.220±0.096	0.173±0.083	0.110±0.064	0.065±0.026	0.079±0.047	0.348±0.285
±SDev	0.276±0.074	0.325±0.066	0.351±0.082	0.345±0.051	0.355±0.077	0.419±0.059	0.347±0.066	0.335±0.075
Median	0.223	0.260	0.205	0.171	0.096	0.057	0.070	0.226
	0.261	0.315	0.366	0.344	0.349	0.419	0.357	0.335
25%	0.158	0.198	0.150	0.122	0.061	0.046	0.048	0.183
	0.221	0.266	0.290	0.305	0.289	0.375	0.295	0.291
75%	0.269	0.326	0.278	0.230	0.149	0.084	0.097	0.427
	0.322	0.384	0.420	0.390	0.436	0.460	0.390	0.387
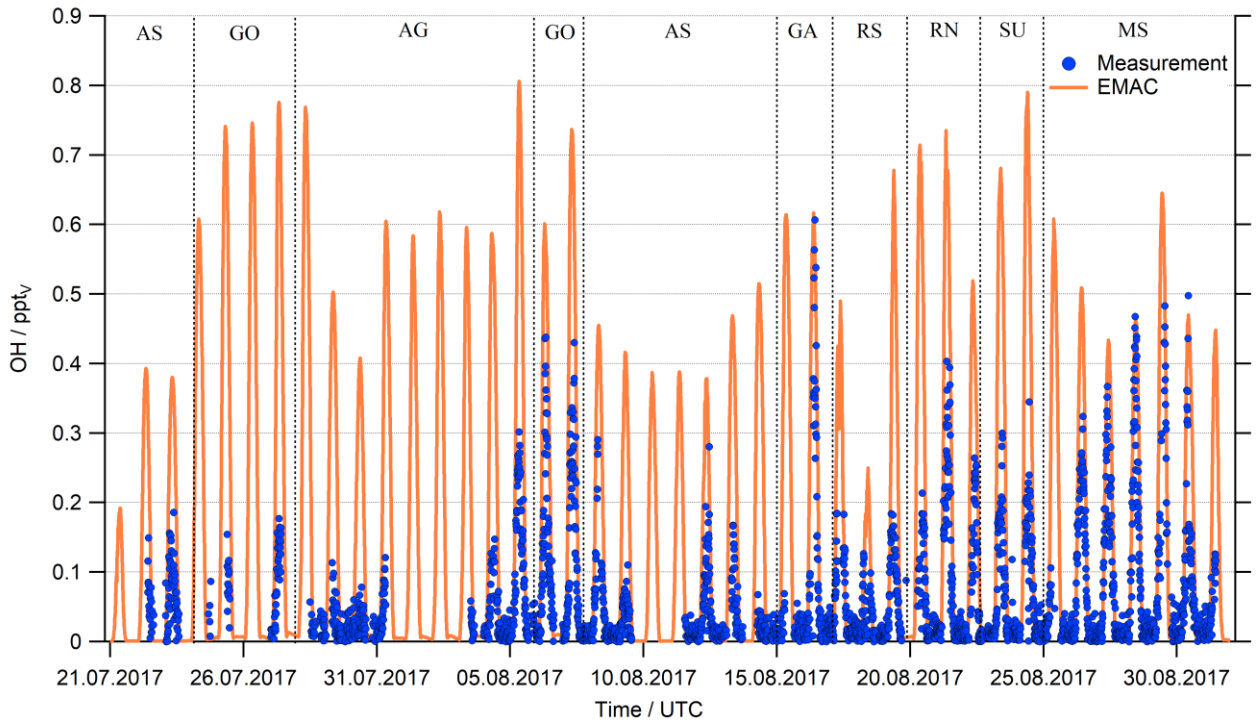
Figure S7: Timelines of the OH measurements and the EMAC simulation, averaged along the ship track.
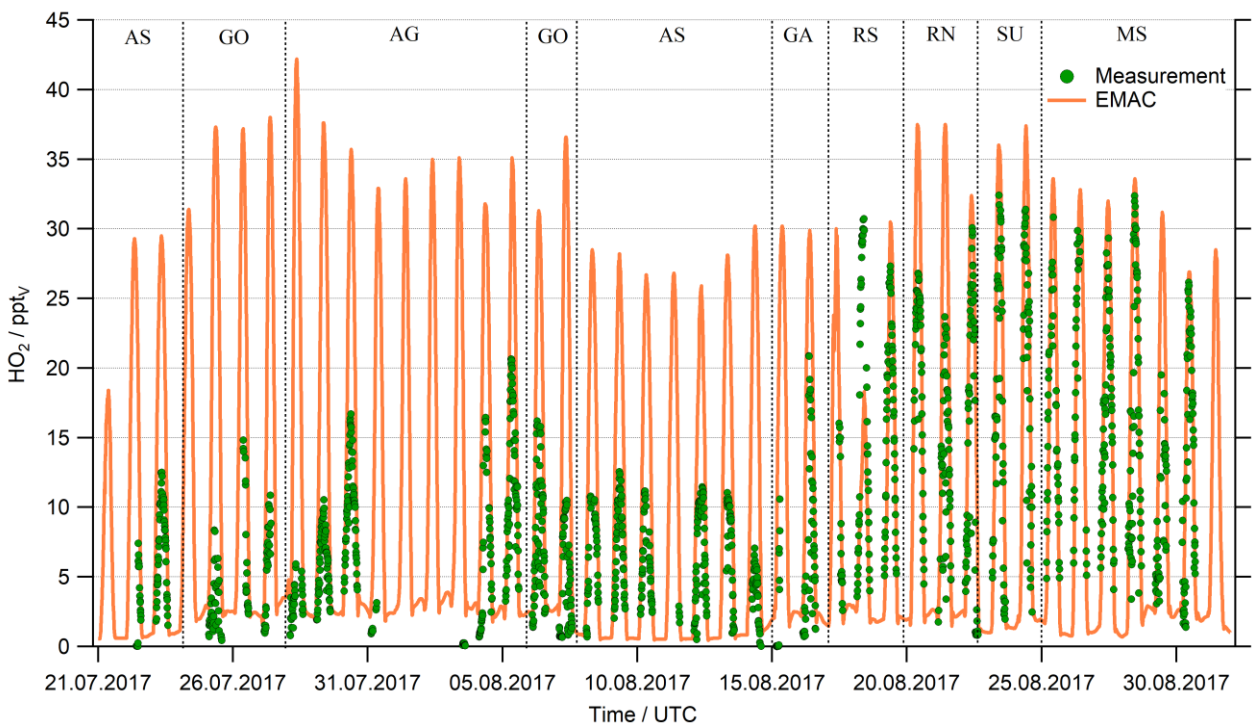
Figure S8: Timelines of the HO₂ measurements and the EMAC simulation, averaged along the ship track.
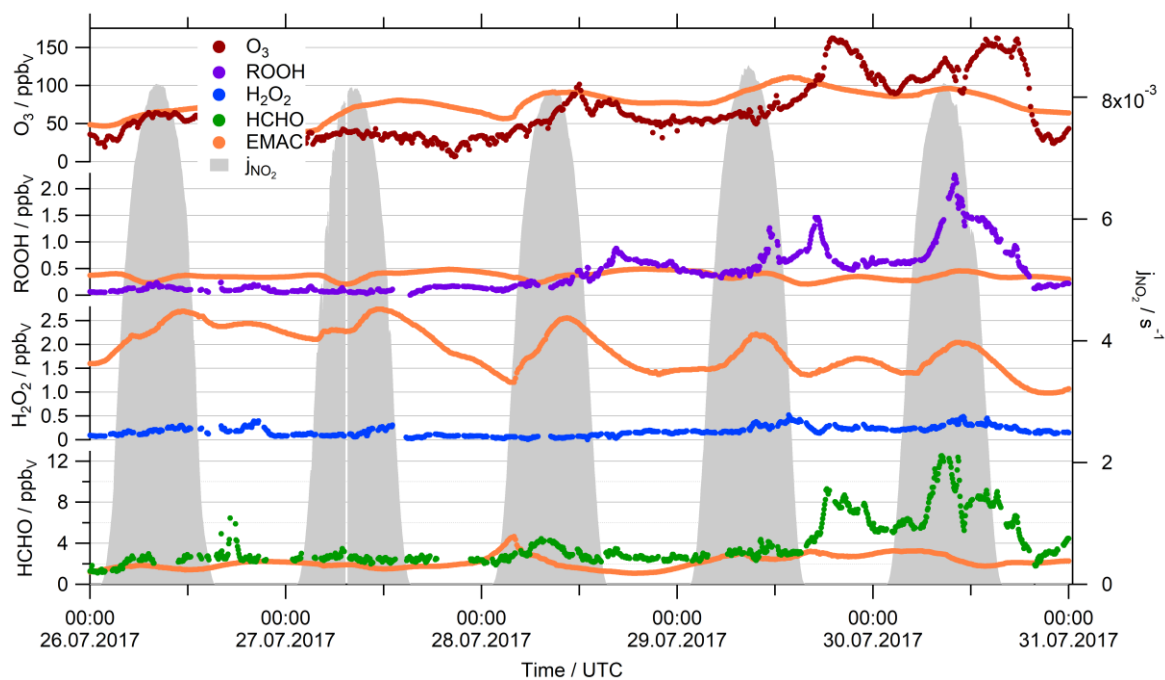
Figure S9: Case study of the Arabian Gulf during the first leg for the observations and the corresponding EMAC simulations. Highly polluted air masses were detected during the night of the 29.07.17, when we measured 170 ppbv of O_3 in the center of the Arabian Gulf.
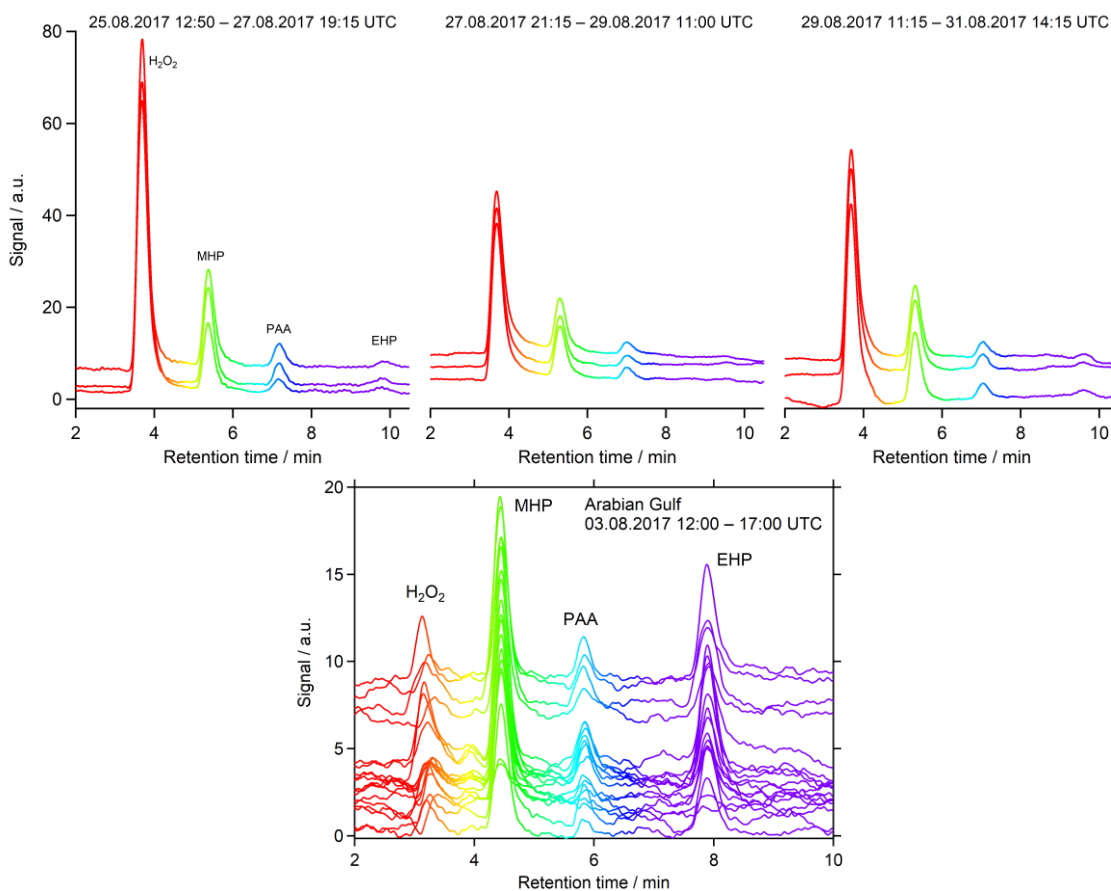
Figure S10: Identification of H_2O_2 and three separated organic peroxides based on the qualitative HPLC measurements. MHP (methyl hydroperoxide), PAA (peracetic acid) and EHP (ethyl hydroperoxide) were identified with their respective retention times and gaseous injections of PAA with a diffusion source. The lower panel shows the continuous results in AG, the upper panel the injection of enriched samples in MS.
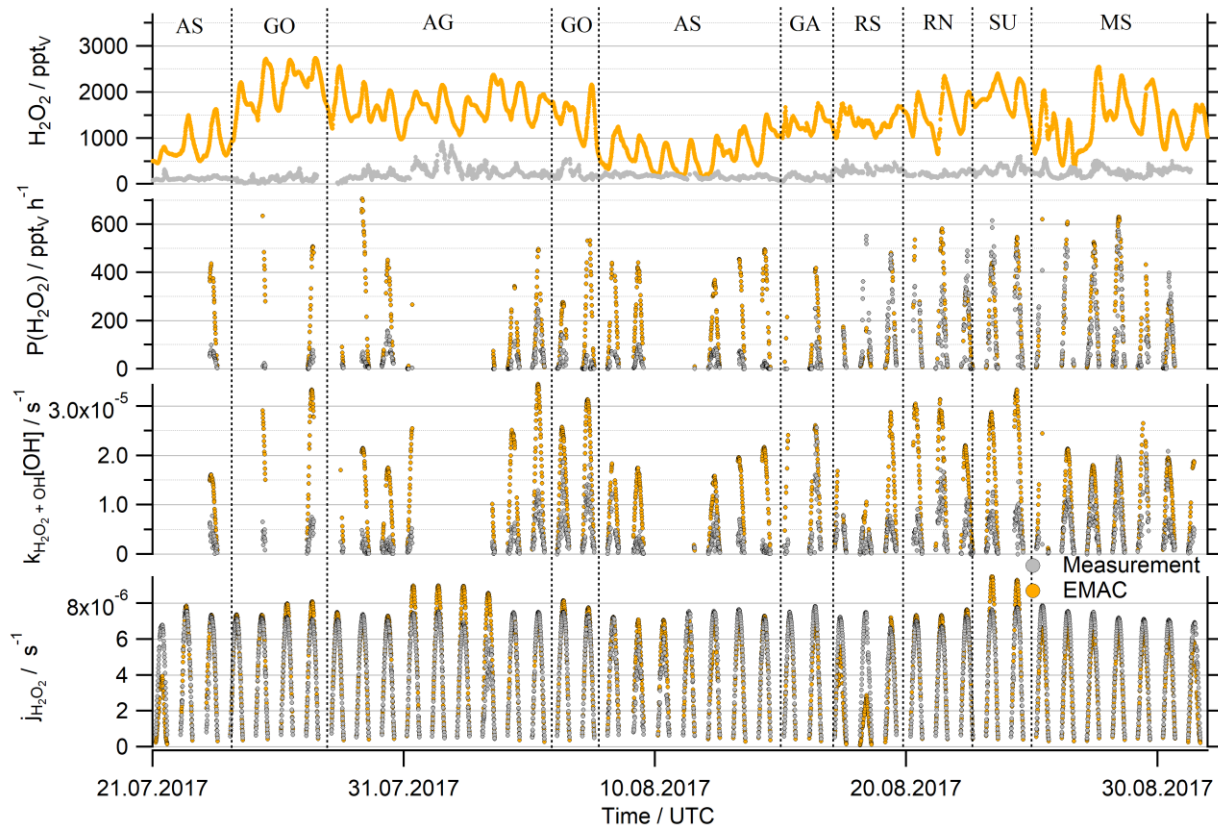
Figure S11: Timelines of the production and loss terms of H₂O₂ for the observations (black) and the EMAC model results (orange). Note that the loss terms were not multiplied with the H₂O₂ mixing ratio.
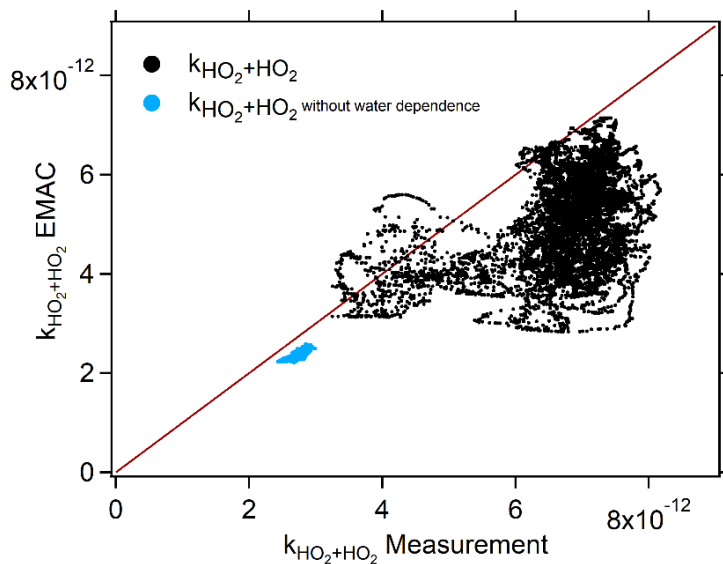
Figure S12: Scatter plot of k_{HO2+HO2} for the measurements and EMAC. The water dependence causes a maximum deviation of about factor 2, as EMAC slightly underestimated water vapor.
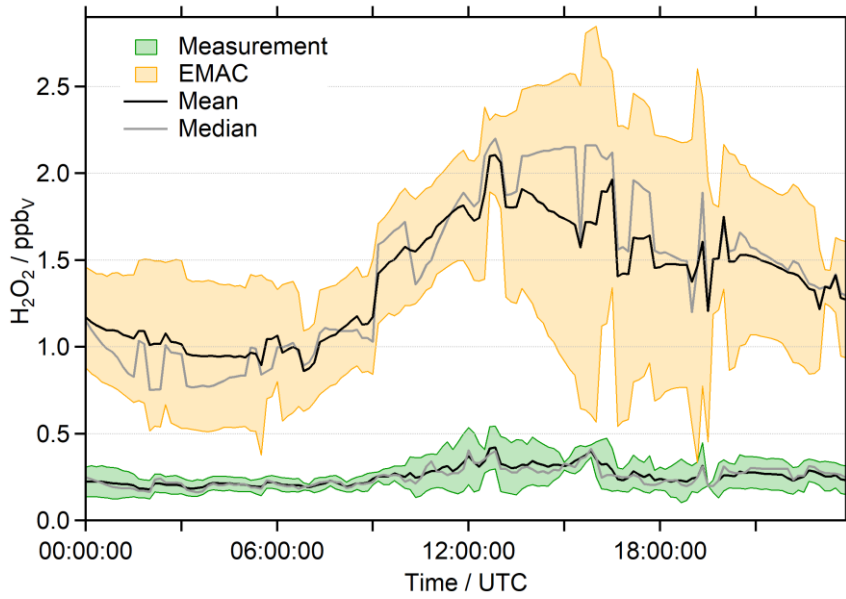
Figure S13: Diurnal variation of H₂O₂ (± 1σ) over the Mediterranean Sea (MS) for the observations (green) and EMAC (orange).
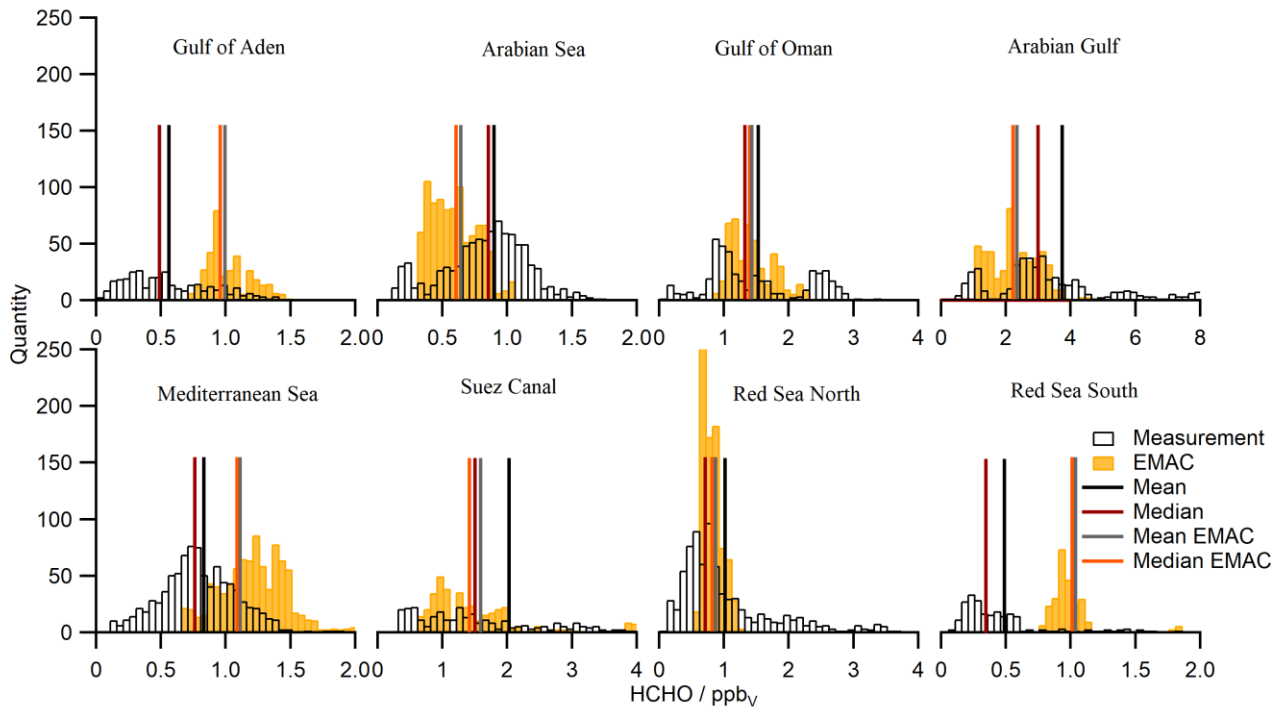
Figure S14: Frequency distributions of the HCHO observations (black) and the EMAC model results (orange) for the eight regions encountered during AQABA.
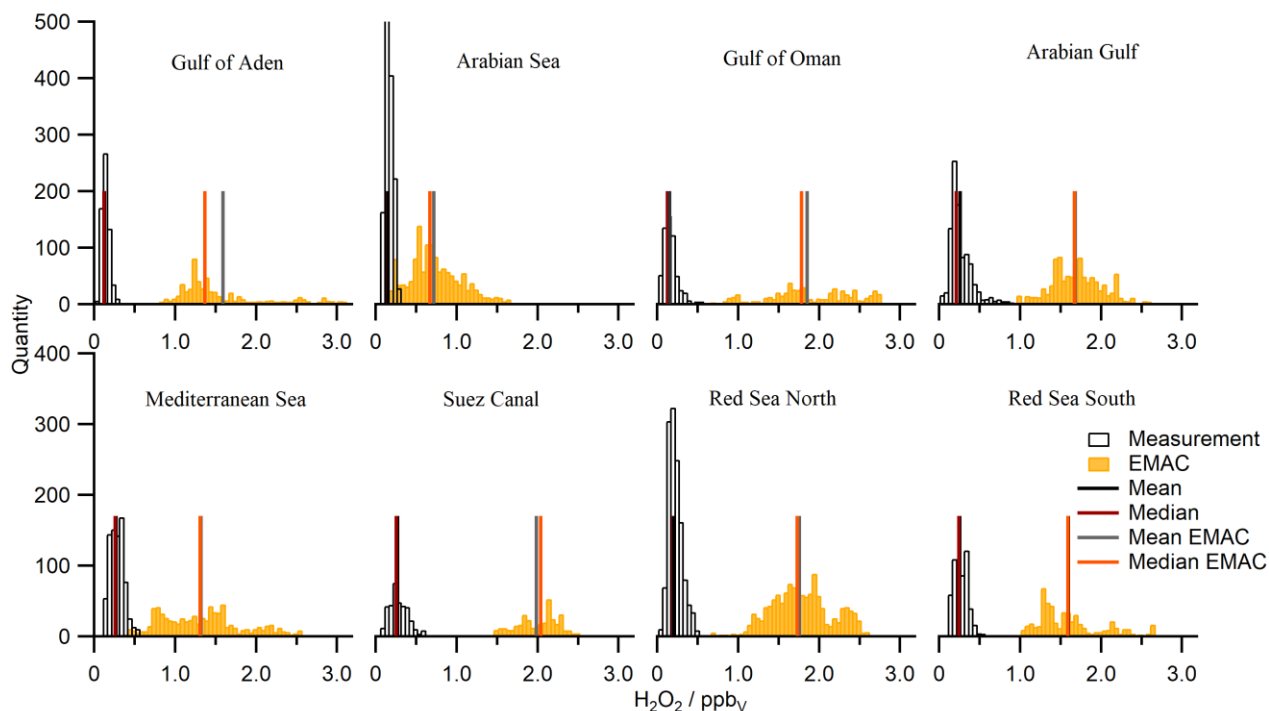
Figure S15: Frequency distributions of the H₂O₂ observations (black) and the EMAC model results (orange) for the eight regions encountered during AQABA.
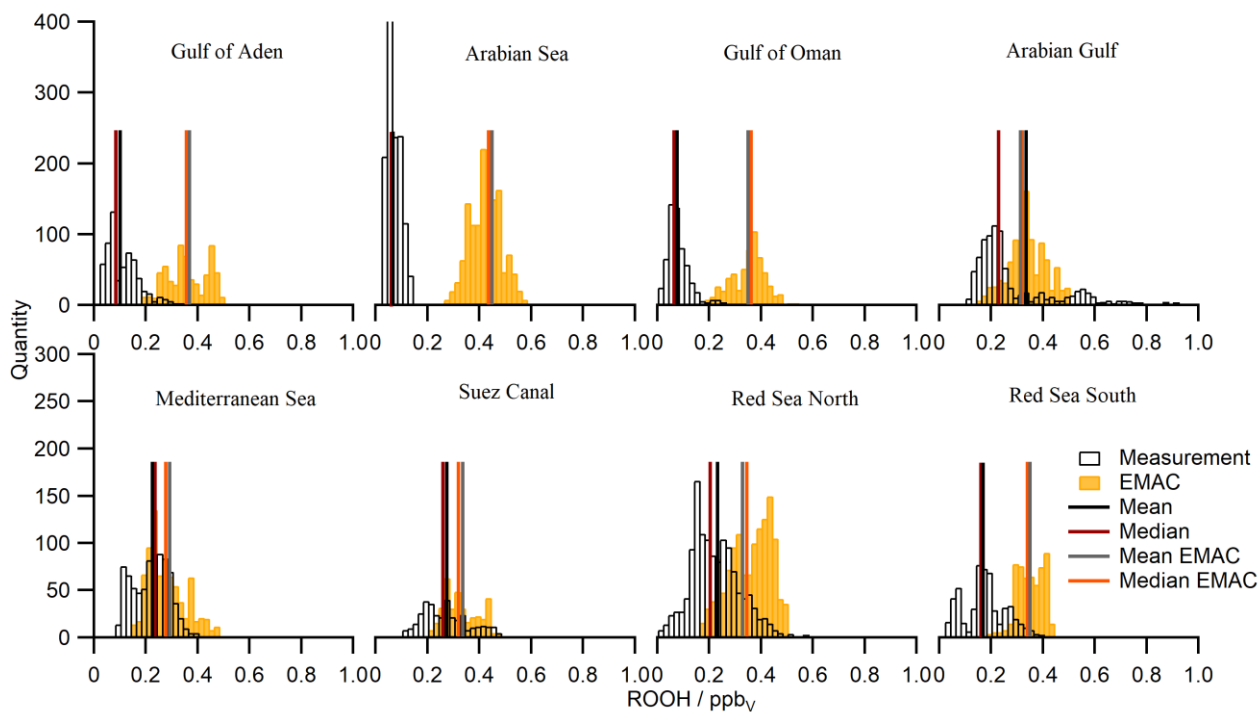
Figure S16: Frequency distributions of the ROOH observations (black) and the EMAC model results (orange) for the eight regions encountered during AQABA.

Table S2: Calculated deposition rates (k_{Dep}) of HCHO and H_2O_2 for the Arabian Sea (AS) and the Mediterranean Sea (MS). Values of k_{Dep} were determined as the slope of a linear regression (logarithmic decay versus time, Fig. 10) and the corresponding deposition velocities (V_{Dep}) are based on Eq. 12 with values for the boundary layer height derived from the ERA5 results for the corresponding timeframe ($\pm 1\sigma$). Errors of k_{Dep} and V_{Dep} are estimated to be at least $\pm 40\%$

	k_{Dep} HCHO / s^{-1}	R^2	V_{Dep} HCHO / cm s^{-1}	k_{Dep} H_2O_2 / s^{-1}	R^2	V_{Dep} H_2O_2 / cm s^{-1}	h_{BL} ERA5 / m
07. - 08.08.17	$1.75 \pm 0.70 \cdot 10^{-5}$	0.69	0.99 ± 0.40	$1.18 \pm 0.47 \cdot 10^{-5}$	0.65	0.67 ± 0.27	569 ± 12
08. - 09.08.17	$1.42 \pm 0.57 \cdot 10^{-5}$	0.47	0.66 ± 0.26	$1.91 \pm 0.76 \cdot 10^{-5}$	0.86	0.89 ± 0.36	465 ± 27
09. - 10.08.17	$0.72 \pm 0.29 \cdot 10^{-5}$	0.42	0.37 ± 0.15	$0.42 \pm 0.17 \cdot 10^{-5}$	0.70	0.22 ± 0.09	520 ± 18
10. - 11.08.17	$0.91 \pm 0.36 \cdot 10^{-5}$	0.68	0.52 ± 0.21	$1.25 \pm 0.50 \cdot 10^{-5}$	0.96	0.71 ± 0.28	573 ± 19
11. - 12.08.17	$2.18 \pm 0.87 \cdot 10^{-5}$	0.64	1.22 ± 0.49	$3.28 \pm 1.31 \cdot 10^{-5}$	0.91	1.83 ± 0.73	559 ± 18
12. - 13.08.17	$1.39 \pm 0.56 \cdot 10^{-5}$	0.59	0.82 ± 0.33	$2.72 \pm 1.09 \cdot 10^{-5}$	0.88	1.59 ± 0.64	586 ± 41
13. - 14.08.17	$1.18 \pm 0.47 \cdot 10^{-5}$	0.44	0.57 ± 0.23	$2.36 \pm 0.94 \cdot 10^{-5}$	0.82	1.14 ± 0.46	483 ± 93
14. - 15.08.17	$1.21 \pm 0.48 \cdot 10^{-5}$	0.52	0.99 ± 0.40	$1.49 \pm 0.60 \cdot 10^{-5}$	0.91	1.22 ± 0.49	822 ± 100
Mean AS ($\pm 1\sigma$)	$1.34 \pm 0.46 \cdot 10^{-5}$	0.56	0.77 ± 0.29	$1.83 \pm 0.93 \cdot 10^{-5}$	0.84	1.03 ± 0.52	572 ± 110
24. - 25.08.17	-	-	-	$0.95 \pm 0.38 \cdot 10^{-5}$	0.58	0.86 ± 0.34	906 ± 68
25. - 26.08.17	-	-	-	$2.87 \pm 1.15 \cdot 10^{-5}$	0.87	2.34 ± 0.94	814 ± 59
26. - 27.08.17	$2.20 \pm 0.88 \cdot 10^{-5}$	0.70	1.76 ± 0.70	$2.30 \pm 0.92 \cdot 10^{-5}$	0.67	1.84 ± 0.74	800 ± 63
27. - 28.08.17	$2.74 \pm 1.10 \cdot 10^{-5}$	0.56	2.22 ± 0.89	$1.68 \pm 0.67 \cdot 10^{-5}$	0.82	1.36 ± 0.54	810 ± 70
28. - 29.08.17	$2.31 \pm 0.92 \cdot 10^{-5}$	0.39	1.86 ± 0.74	$1.16 \pm 0.46 \cdot 10^{-5}$	0.54	0.94 ± 0.38	808 ± 35
29. - 30.08.17	$1.97 \pm 0.79 \cdot 10^{-5}$	0.73	1.39 ± 0.56	$1.22 \pm 0.49 \cdot 10^{-5}$	0.58	0.86 ± 0.34	706 ± 47
30. - 31.08.17	$0.33 \pm 0.13 \cdot 10^{-5}$	0.39	0.23 ± 0.09	$0.39 \pm 0.15 \cdot 10^{-5}$	0.45	0.26 ± 0.10	715 ± 68
Mean MS ($\pm 1\sigma$)	$1.91 \pm 0.93 \cdot 10^{-5}$	0.55	1.49 ± 0.76	$1.51 \pm 0.85 \cdot 10^{-5}$	0.66	1.21 ± 0.69	792 ± 74
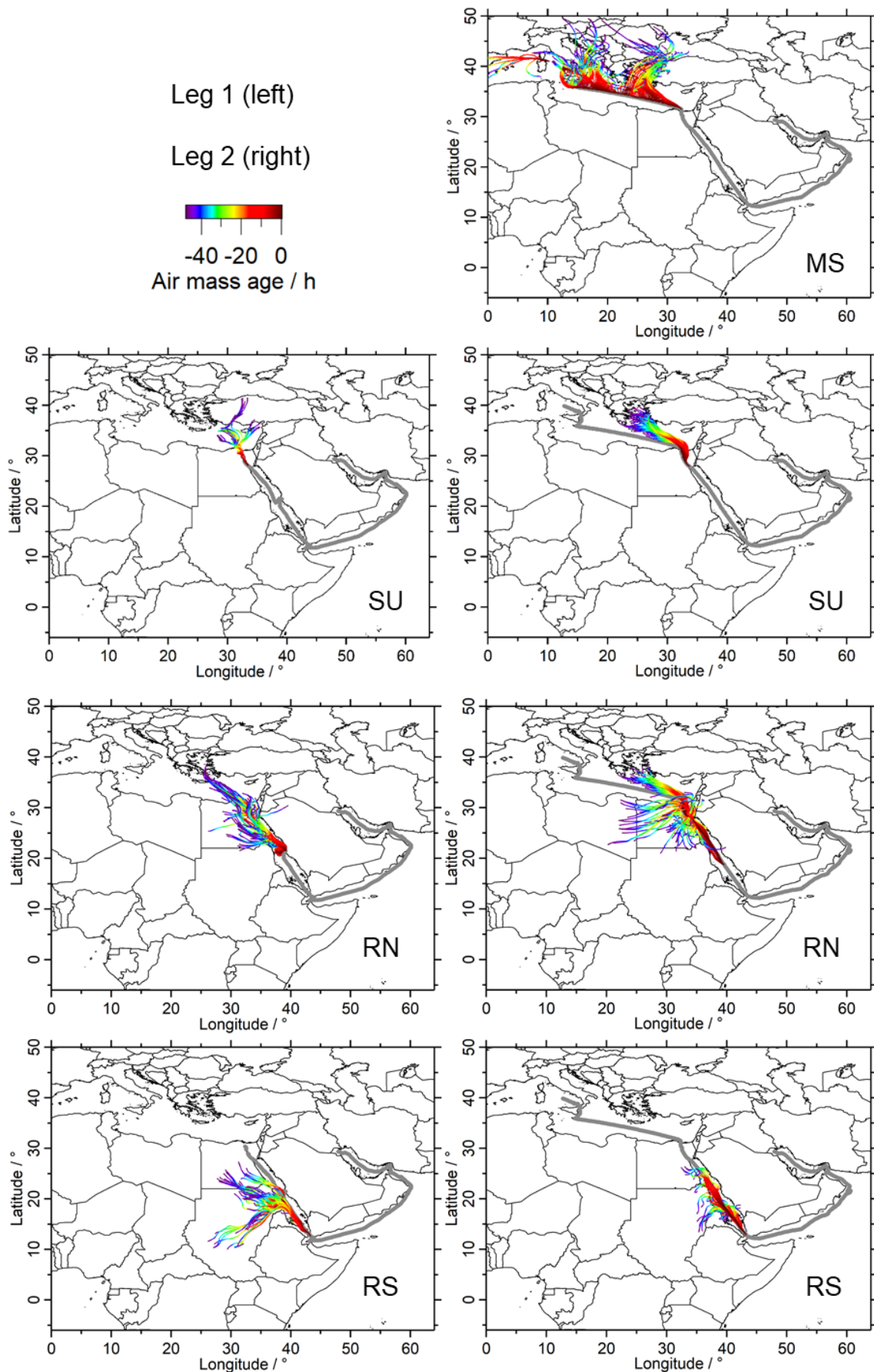
Figure S17: HYSPLIT trajectories for the Mediterranean Sea (MS), the Suez Canal and the Gulf of Suez (SU), the northern Red Sea (RN) and the southern Red Sea (RS) starting with a sampling height of 200 m, with a resolution of 1 h and 48 h of air mass transport. The first leg is shown on the left and the second leg of AQABA on the right.
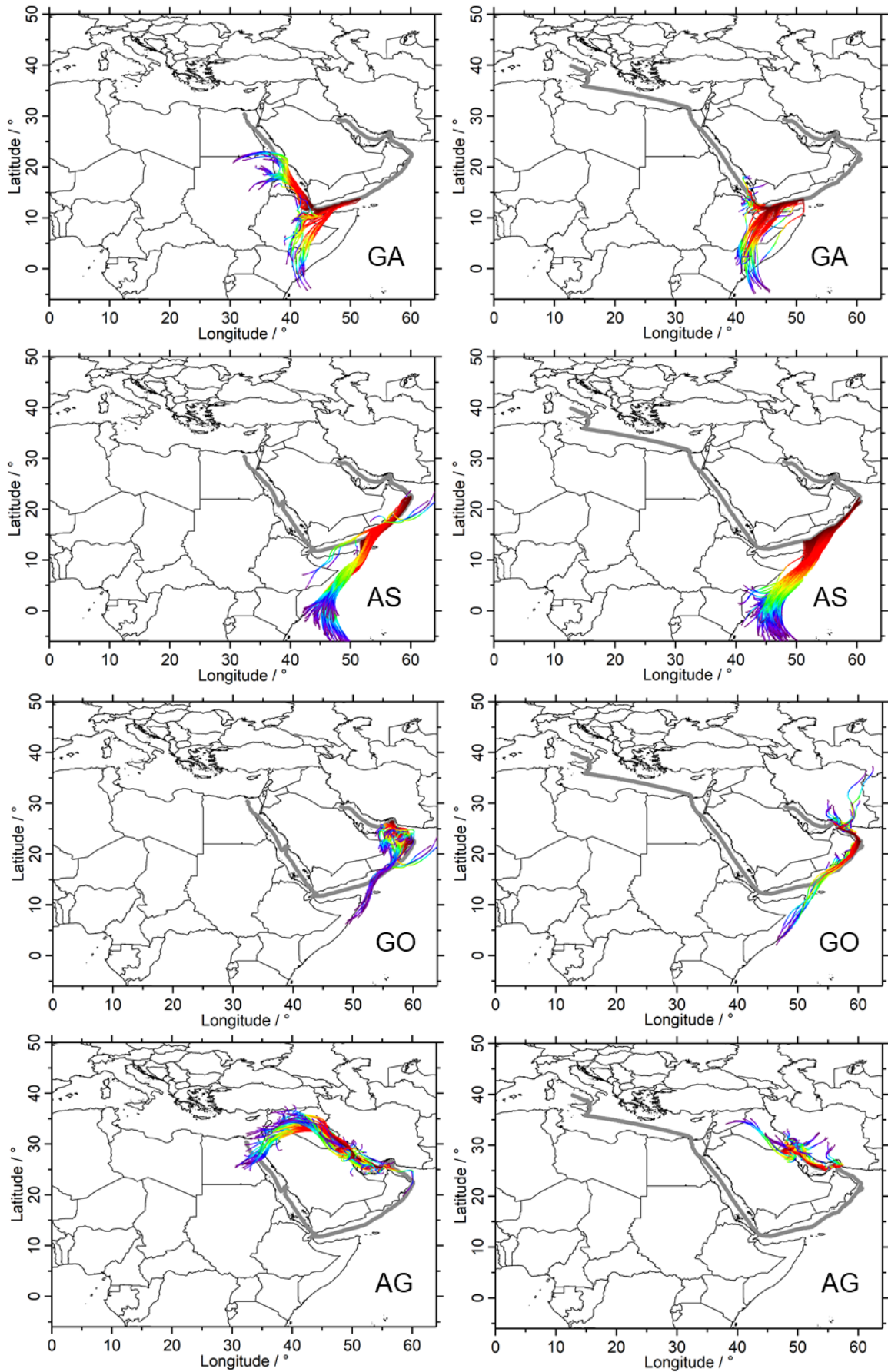
Figure S18: HYSPLIT trajectories for the Gulf of Aden (GA), the Arabian Sea (AS), the Gulf of Oman (GO) and the Arabian Gulf (AG) starting with a sampling height of 200 m, with a resolution of 1 h and 48 h of air mass transport. The first leg is shown on the left and the second leg of AQABA on the right.
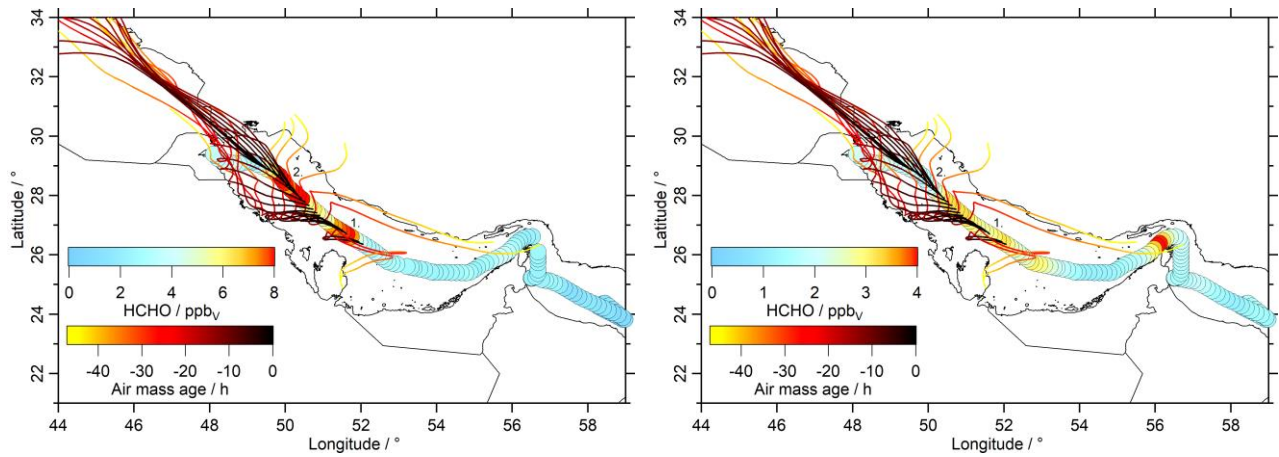
Figure S19: HCHO observations (left) and EMAC results (right) in hourly averages during the first leg over the Arabian Gulf. HYSPLIT trajectories indicate air masses originating in Qatar during the first pollution event (1.) with up to 9 ppbv HCHO and even higher mixing ratios during the second event (2.) with up to 12 ppbv HCHO in air masses originating in Iraq. EMAC simulates elevated HCHO in these air masses with up to 3 ppbv, although it did not match the observations. Paris et al. (2021) identified natural gas flaring as a major source for the elevated VOCs in the region.